Bulletin of the Seismological Society of America, in press 2003

Structure and mechanics of the Hayward-Rodgers Creek fault stepover, San Francisco Bay, California

By Tom Parsons, Ray Sliter, Eric L. Geist, Robert C. Jachens, Bruce E. Jaffe, Amy Foxgrover, Patrick E. Hart, and Jill McCarthy *U.S. Geological Survey, Menlo Park, CA*

Abstract. A dilatational stepover between the right-lateral Hayward and Rodgers Creek faults lies beneath San Pablo Bay in the San Francisco Bay area. A key seismic hazard issue is whether an earthquake on one of the faults could rupture through the stepover, enhancing its maximum possible magnitude. If ruptures are terminated at the stepover, then another important issue is how strain transfers through the step. We developed a combined seismic reflection and refraction cross-section across south San Pablo Bay and found that the Hayward and Rodgers Creek faults converge to within 4 km of one another near the surface, about 2 km closer than previously thought. Interpretation of potential field data from San Pablo Bay indicated low likelihood of strike-slip transfer faults connecting the Hayward and Rodgers Creek faults. Numerical simulations suggest that it is possible for a rupture to jump across a 4-km fault gap, though special stressing conditions are probably required (e.g., Harris and Day, 1993; 1999). Slip on the Hayward and Rodgers Creek faults is building an extensional pull-apart basin that could contain hazardous normal faults. We investigated strain in the pull-apart using a finite element model, and calculated a ~0.02 MPa/yr differential stressing rate in the stepover on a least-principal-stress orientation nearly parallel to the strike-slip faults where they overlap. A 1-10 MPa stress-drop extensional earthquake is expected on normal faults oriented perpendicular to the strike-slip faults every 50-500 years. The last such earthquake might have been the 1898 **M**=6.0-6.5 shock in San Pablo Bay that apparently produced a small tsunami. Historical hydrographic surveys

gathered before and after 1898 indicate abnormal subsidence of the Bay floor within the stepover, possibly related to the earthquake. We used a hydrodynamic model to show that a dip-slip mechanism in north San Pablo Bay is the most likely 1898 rupture scenario to have caused the tsunami. While we find no strike-slip transfer fault between the Hayward and Rodgers Creek faults, a normal-fault link could enable through-going segmented rupture of both strike-slip faults, and may pose an independent hazard of **M**~6 earthquakes like the 1898 event.

Introduction

The Hayward and Rodgers Creek faults accommodate significant right-lateral North America-Pacific plate boundary strain east of San Francisco Bay (~9 mm/yr; Working Group on California Earthquake Probabilities, 1999), and are the likely site of the 1868 **M**=6.8, and 1898 **M**=6.3 earthquakes (Toppozada et al., 1992; Bakun, 1999). The two faults emerge from San Pablo Bay, the Hayward fault to the south and the Rodgers Creek to the north (Fig. 1), and have been assigned the highest **M**>6.7 earthquake probability in the San Francisco Bay region. The trends of the two faults are offset about 5-6 km, with the Rodgers Creek lying east of the Hayward fault, apparently making an dilatational step under San Pablo Bay (Fig. 1).

The structure of the stepover remains mysterious. A solution to the mystery is important because if the two faults are joined at depth, then the combination of the ~90-km-long Hayward fault with the ~60-km-long Rodgers Creek fault might generate a **M**~7.6 earthquake instead of **M**~7.2 and **M**~7.0 earthquakes on each of the shorter segments (e.g., Wells and Coppersmith, 1994). This uncertainty requires multiple segmentation models to be applied in hazard analysis (e.g., Working Group on California Earthquake Probabilities, 1999). If the stepover is a barrier to

rupture, then the mechanism that passes strain from the Hayward to the Rodgers Creek fault must be investigated for seismic potential.

Uncertainty about a connection between the Hayward and Rodgers Creek faults is the result of the junction being under the very shallow water of San Pablo Bay, making surface geological study impossible, and subsurface geophysical studies difficult. Perhaps the most comprehensive study was conducted by Wright and Smith (1992), who interpreted proprietary gravity, seismic, and well data within the stepover. In two cross-sections across northern and central San Pablo Bay, Wright and Smith (1992) showed that the Rodgers Creek fault lies at least 6 km east of the Hayward fault, and dips steeply down to the east; from these sections it was concluded that through-going rupture is unlikely. In this study we provide an additional structural cross section across southern San Pablo Bay, which allows us to build on the results of Wright and Smith (1992) by placing limits on the southern extent of the Rodgers Creek fault. In addition, we identify the nearest approach of the Rodgers Creek fault to the Hayward fault to be ~4 km; because this step is wide, we model the kinematics of the stepover zone using a finite element technique, and we study the mechanics of an historical earthquake (1898) that occurred in or near the stepover.

Seismic Transect: South San Pablo Bay

Data collection and processing

We drew a revised fault map for the Hayward-Rodgers Creek stepover by interpreting a new seismic transect that crosses southern San Pablo Bay (Figs. 1,2,3). The cross-section was developed by combining a high-resolution vertical incidence reflection section with a coincident 2-D tomographic velocity model.

Reflection data were collected in 1994 with a multichannel seismic system capable of imaging geologic structures to 1- to 2-km depth with a spatial resolution of 5 to 10 m in relatively shallow water environments (Childs et al., 2000). The main components of this system were a small airgun source, a short 24-channel streamer, and a compact PC-based digital recording instrument. The streamer was 150 m long, with a 6.25-m group interval and one hydrophone per channel. The source was a pair of 0.65 L airguns with "wave shape" kits installed in their chambers to suppress the bubble pulse. Resulting common-midpoint data were either 12- or 6-fold, with a 3.125-m common-midpoint interval. Data were recorded at a 1-ms sample interval to a 2 s record length. The data-processing sequence used to create stacked profiles from the field data is resampling to 2 ms, trace edit, geometry assignment, bandpass filter (50-200 Hz), automatic gain control (100 ms window), water-bottom mute, frequency-wavenumber filter (50-200 Hz; ±2,400 m/s), spiking deconvolution, common-midpoint sort, stacking-velocity analysis, normal-moveout correction, and stack. Data quality from San Pablo Bay is highly variable because of prevalent shallow gas deposits. We found that overlaying the data on a coincident seismic velocity cross-section enhanced our ability to interpret them.

A 2-D tomographic velocity model across San Pablo Bay was calculated from first arrival times on shot gathers from a deep-crustal seismic reflection experiment conducted in 1991, the

Bay Area Seismic Imaging experiment (BASIX). BASIX was the first attempt to use marine seismic-reflection profiling to define the deep-crustal structure and fault geometry of the San Francisco Bay region. Because heavy ship traffic, shallow water, and strong tidal currents combined to make the use of a conventional kilometers-long towed hydrophone streamer unfeasible, individual floating hydrophones with radio telemetry units were used as receivers. These receivers were anchored at 100- to 200-m intervals adjacent to the ship tracklines to record airgun blasts**.** The airguns were fired at 50-m intervals along the receiver array and off end to distances of approximately 20 km. Deep reflection data quality were poor in San Pablo Bay because of noise from tidal currents and strong winds, and these data are not useful for direct imaging of faults. However, the first arrivals are generally of good quality, and because of the ~20-km offsets, these data can be utilized for refraction velocity analysis.

We employed a 2-D tomographic inversion of first arrival times (Parsons et al., 1996) that uses a finite-difference travel-time technique developed by Vidale (1990) to perform accurately in the presence of large velocity contrasts. Ray paths were computed by following the gradient in travel-time from the receiver to the source. We used a Laplacian smoothness criterion (Lees and Crosson, 1989) and solved for velocity perturbations using the LSQR algorithm of Paige and Saunders (1982). A total of 18695 traveltimes recorded on 128 receivers were hand picked from receiver gathers, and inverted for velocity structure on 50x50-m cells. The RMS traveltime misfit was reduced to less than 0.1 s (estimated picking error) after 6 iterations.

Interpretation and fault map of the Hayward-Rodgers Creek stepover

A cross-section of the upper 2 km across south San Pablo Bay (Fig. 1) shows clear evidence for active and recent faulting (Fig. 2). A sharp lateral discontinuity in velocity structure and sedimentary layering is obvious about 1 km east of the currently active trace of the Hayward fault, with lower velocities and more distinct layering occurring to the east. This transition may represent an historic trace of the Hayward fault. A very subtle velocity low corresponds to the current trace of the Hayward fault, which otherwise shows no signature on the cross-section, perhaps an indication that the historic trace to the east was active for a longer time than the current trace has been, although the current trace bounds a prominent magnetic anomaly (Jachens et al., 2002).

About 4 km east of the current Hayward fault there is another significant discontinuity which separates east-dipping bedding from west-dipping layers, and which is associated with disrupted sediments at and near the surface. This fault appears to dip steeply down to the east and is on the projected trend of the southernmost Rodgers Creek fault, as defined by Wright and Smith (1992). We thus extended the Rodgers Creek fault south to the location of the cross-section in south San Pablo Bay (Fig. 3). Wright and Smith (1992) also identified an east branch off the southern Rodgers Creek fault (Fig. 3), which does not appear to reach our south San Pablo Bay cross section. East of the Rodgers Creek fault is a ~6 to 8-km-wide, gently west-dipping sedimentary basin, which appears to be truncated by the fault.

Shallow sediments are deformed about 8 km east of the active Hayward fault (4 km east of the Rodgers Creek). This deformation was attributed to the offshore extension of the Pinole fault, an active, east-dipping thrust, by Anima et al. (1992) and Wright and Smith (1992). We thus

extended the Pinole fault offshore as far as the south San Pablo Bay cross section (Fig. 3), but not much farther because the Pinole fault was not identified by Wright and Smith (1992) on either the central or northern San Pablo Bay sections.

A very limited number of microearthquakes occur in San Pablo Bay, which makes projection of near-surface features difficult. Hypocenters relocated using the double difference technique (Waldhauser and Ellsworth, 2002) are shown on Figure 2. These scant events are not inconsistent with the structural cross-section; there is a cluster that appears to line up with the deeper projection of the east-dipping Rodgers Creek fault, though we are hesitant to make any conclusions from so few events. The available catalog focal mechanisms from the Hayward-Rodgers Creek stepover show almost no right-lateral solutions parallel to the major faults; instead, they are right-lateral on perpendicular subfaults, or are left lateral events (Fig. 4). A few events have oblique dip-slip solutions. With such limited and highly variable solutions, it is difficult to determine the seismotectonics of the stepover. We instead apply a variety of data sources and modeling techniques to learn more about strain within the stepover.

Potential field data: San Pablo Bay

Observations and interpretation based on gravity data

We analyzed potential field data to support the seismic modeling and to search for evidence of any linking faults between the Hayward and Rodgers Creek faults. A detailed gravity survey was conducted around and on the bottom of San Pablo Bay in 1967 (Wright and Smith, 1992), the data of which we recovered from original contour maps at survey locations. A filtered version of these data is shown in Figure 5, which represents the difference between the gravity

field measured at the ground surface, and those same data upward continued (mathematically transformed to a level) 500m above the ground surface. Upward continuation suppresses the shorter-wavelength components of a gravity anomaly, such as those produced by the shallowest parts of a body, at the expense of the longer-wavelength components that reflect the deeper parts of the body (Blakely, 1995). By viewing the difference between the data and the upward-continued data, we focus on the parts of the anomalies produced by the shallowest density distributions. The purpose of this filtering is to examine approximately the same parts of the crust as the seismic cross-section shown in Figure 2.

San Pablo Bay is characterized by a strong gravity low (up to 38 mGal) associated with a deep (up to 8 km) sedimentary basin (Wright and Smith, 1992), which is also apparent in the filtered data (Fig. 5). The gravity low is bounded to the west by the Hayward fault zone, with the strongest gradient corresponding to the historic trace identified in the seismic cross-section (Fig. 2), rather than the active trace located ~1 km to the west. A similar gradient is seen trending southwest-northeast across northern San Pablo Bay between the Hayward and Rodgers Creek faults (Fig. 5). The Rodgers Creek fault itself is not associated with any gravity signature in San Pablo Bay (Wright and Smith, 1992), though on the filtered data plot there appears to be slightly lower gravity values between the Hayward and Rodgers Creek faults than elsewhere in the Basin. This gravity low might be an indication of most recent subsidence and younger, less consolidated sediments relative to the rest of the basin.

Observations and interpretation based on aeromagnetic data

High-resolution aeromagnetic surveys of the San Pablo Bay area and vicinity were flown on contract to the U.S. Geological Survey during the Fall of 1991 and March 1995. Total field

magnetic data were collected with a fixed-wing aircraft along NE-SW oriented flightlines spaced 500 m apart. The survey aircraft maintained a nominal height of 250 m above the surface in water-covered areas and 300 m above the land surface in developed onshore areas. Data were collected about every 50 m along the flight lines. The magnetic data were corrected for diurnal fluctuations of the Earth's field, and the International Geomagnetic Reference Field (Langel, 1992), updated to the dates of the survey, was subtracted from the observations to yield residual magnetic data (total field magnetic anomaly). The residual magnetic field values were interpolated to a square grid of 0.1x0.1 km intervals and interpreted by Jachens et al. (2002) (Fig. 6).

North of San Pablo Bay and adjacent to the Rodgers Creek fault, a high-amplitude, southeast trending magnetic high reflects a magnetic source body, most likely composed of Tertiary volcanic rocks (Wright and Smith, 1992). The continuation of this magnetic anomaly beneath San Pablo Bay indicates that the source body bends to the south and ultimately truncates against the active trace of the Hayward Fault between 8 and 13 km northwest of Pinole Point (Fig. 6). The continuity of this magnetic source body precludes any direct fault connection between the upper parts of the Hayward and Rodgers Creek Faults north of the south edge of this body because any such fault that accommodated significant strike-slip offset would necessarily have offset the magnetic source body (Jachens et al., 2002). More limited offset of the magnetic anomaly beneath San Pablo Bay could have occurred near the north shore of the Bay, where there is a southwest-northeast trending boundary of the anomaly that is coincident with a gravity gradient of similar trend (Figs. 5, 6). Another potential boundary lies at the south edge of the anomaly near the southern extent of the Rodgers Creek fault (Fig. 6), though this boundary does not have a corresponding gravity signature (Fig. 5).

In summary, analysis of the potential field data tells us that the least dense sediments lie between the Hayward and Rodgers Creek faults, and by inference, that the most recent subsidence occurs there. The breadth of the gravity anomaly in San Pablo Bay suggests that some form of fault-related subsidence has occurred over an extended time, and that the focus of peak subsidence changed with time. Aeromagnetic anomalies trend across the stepover that are uncut by faults, suggesting that there is no strike-slip link between the Hayward and Rodgers Creek faults. If there is no strike-slip link, then strain must be accommodated some other way. The question that arises from analysis of seismic and potential field data is: are there other types of faults that could enable a through-going rupture, or if not, does the stepover itself represent a seismic hazard? We employ a variety of modeling techniques and historic observations to gain insight into these questions.

Stressing implications and transfer of strain through the Hayward-Rodgers Creek fault stepover from finite element modeling

The goal of this study is to determine how seismic strain is transferred through the Hayward-Rodgers Creek fault stepover. Evidence from seismic transects and potential field data indicate that the Hayward and Rodgers Creek faults overlap, approach within 4 km of one another, but do not have a direct strike-slip connection in the upper crust beneath San Pablo Bay. We thus investigate other possible seismic strain modes. Because the two right-lateral faults form a right step, the crust between them is subject to extensional stress as the faults accumulate ~9 mm/yr of right-lateral slip, which appears to have generated a pull-apart basin. We constructed a 3-D finite element model using the new fault map shown in Figure 3 to investigate the magnitude, rate,

orientation, and distribution of extensional stresses expected to result from the stepover geometry beneath San Pablo Bay. Using these results we can look for the structures that accommodate them.

Finite element model construction

The elastic part of the crust (upper 15 km) was simulated with 8-node, extruded tetrahedral elements (Fig. 7). The constitutive properties of the crust were approximated by those of wet Westerly granite, and characterized by three elastic parameters: a Young's modulus of $E = 8 \cdot 10^4$ MPa, a density of $\rho = 2.7 \cdot 10^3 kg \cdot m^{-3}$, and a Poisson's ratio of $\nu = 0.25$. The model was oriented parallel to the average trend of the Hayward and Rodgers Creek faults, and extends 40 km perpendicular to the faults and 70 km along strike.

The finite element model has vertical cuts in it that represent the Hayward and Rodgers Creek faults (Fig. 7). The faults are deformable, and are constructed from contact elements that obey the Coulomb failure relation

$$CF \equiv \tau_f + \mu(\sigma_n) \tag{1}$$

where τ_f is the shear stress acting on a fault surface, μ is the friction coefficient, and σ_n is the component of stress acting normal to a fault surface (pore fluid pressures were assumed constant and hydrostatic). Contact elements have zero thickness and are welded to the sides of the solid model elements. The model block west of the Hayward and Rodgers Creek faults was constrained to move 9 mm/yr (e.g., Working Group on California Earthquake Probabilities,

1999) , while the block east of the faults was held fixed. The free surface was left unconstrained. The bottom of the model was allowed to freely move laterally, but not vertically, simulating an elastic layer overlying a less viscous substrate that, over the long term (many seismic cycles), builds no differential stress. This assumption requires complete decoupling of vertical motions from the lower crust, which is unlikely in the real Earth; however only about 10 m of thinning in the stepover over 20,000 years is predicted by the model, suggesting that vertical motion is likely unimportant to mean stress orientations on that time scale.

All velocity constraints were imposed on the model edges; other than gravity, no constraints were imposed on elements within the model. We held all elastic parameters fixed throughout the modeling, thus the only free parameter was the coefficient of friction on the faults, which can theoretically range from 0 to 1, though most investigators conclude that the strike-slip faults of the San Andreas system have very low (μ=0.1-0.2) friction coefficients (e.g., Lachenbruch and Sass; 1980; Zoback, 1991; Reasenberg and Simpson, 1992; Bird and Kong, 1994; Miller, 1996; Parsons et al., 1999; Geist and Andrews, 2000)

The finite element analysis was conducted using the ANSYS® program. ANSYS® employs the Newton-Raphson approach to solve nonlinear problems. In this method, a load is subdivided into a series of increments applied over several steps. Before each solution, the Newton-Raphson method evaluates the out-of-balance load vector, which is the difference between the restoring forces (the loads corresponding to the element stresses) and the applied loads. A linear solution is performed, using the out-of-balance loads, and checks for convergence. If convergence criteria are not satisfied, the out-of-balance load vector is re-evaluated, the stiffness matrix updated, and a new solution is obtained. The system of equations is solved through direct elimination of equations until the problem converges (sparse direct solver).

Finite element model results

Stressing within the Hayward-Rodgers Creek stepover was simulated by moving the west model edge at 9 mm/yr for 20,000 years after allowing the model to completely compress under its own weight. Models were run with fault friction coefficients of μ=0.1, μ=0.4, and μ=0.8. Fault friction was kept uniform, causing the faults to slip at a constant rate; the cumulative stressing effect on the crust is the same as stick slip behavior provided the model is run for times exceeding multiple seismic cycles. As might be expected, the Hayward fault accommodated all motion south of the stepover, the Rodgers Creek fault accommodated it to the north, and the two faults shared the strain where they overlap in San Pablo Bay (Fig. 7). The small eastern branch of the Rodgers Creek fault mapped in San Pablo Bay by Wright and Smith (1992) (Fig. 3) was built into the model, but it didn't slip because the more continuous faults absorbed all the strain.

In the finite element model, the crust between the Hayward and Rodgers Creek faults was increasingly stressed with increasing fault slip where the two faults overlap beneath San Pablo Bay (Fig. 8). The differential stress state is extensional, with the least principal stress oriented roughly parallel to the Hayward-Rodgers Creek trend (Fig. 8). The model predicts that extensional strain should occur on normal faults oriented roughly orthogonal to the Hayward-Rodgers Creek fault trend. The orthogonal orientation may result from the modeled strike-slip faults having significant overlap (e.g., ten Brink et al., 1996). Gravity and aeromagnetic data show at least one potential basin-crossing normal fault, located in northern San Pablo Bay (Figs. 5, 6).

The finite element simulations allowed us to track the growth of differential stress with time in the Hayward-Rodgers Creek stepover. The stressing rate in the crust between the two faults is calculated to be about 0.02 MPa/yr at 7 km depth, independent of friction coefficient after ~10 ky of slip (Fig. 9). Measured frictional strengths of Hayward fault zone and surrounding rocks range between ~200 and 350 MPa differential stress at 7 km depth (Morrow and Lockner, 2001). Thus the Hayward-Rodgers Creek stepover could theoretically exist for 10-20 ky before extensional faulting would be expected (Fig. 9). Once extensional faults have organized, then earthquakes would be expected to occur on them at intervals of 50-500 years, if they had typical stress drops of 1 to 10 MPa.

Modes of extensional accommodation from analogous modeling and observational studies

From the finite element modeling results we should expect significant extensional strain in the Hayward-Rodgers Creek fault stepover. The seismicity rate is low (Fig. 3), which makes identifying potential normal, or oblique faults difficult. Gravity and magnetic observations can be interpreted to identify at least one possible basin-bounding feature in northern San Pablo Bay (Fig. 5), and suggest that the existence of a strike-slip transfer fault connecting through the stepover is unlikely (Jachens et al., 2002) (Fig. 6). A summary of field observations and modeling studies provides a framework for which modes of extensional accommodation might be expected in a pull-apart basin bounded by overlapping strike-slip faults.

Pull-apart basins are commonly found at releasing steps between en echelon strike-slip faults (e.g., Sylvester, 1988), typically have rhombic shapes in map view, and are often bounded by high-angle normal or oblique faults (e.g., Mann et al., 1983). The angle between bounding

normal and strike-slip faults varies, and may depend on the frictional strength and degree of overlap of the strike-slip faults (Ben-Avraham and Zoback, 1992; ten Brink et al., 1996). Pull-apart basins may be symmetric or asymmetric; the degree of symmetry may be controlled by the relative coupling between the bounding strike-slip faults and the intervening crust (e.g., Rahe et al., 1998). In the finite element model presented here, coupling was uniform, and a symmetric differential stress field was produced (Fig. 8).

The evolution and development of pull-apart basins has been investigated using analog modeling (e.g., McClay and Dooley, 1995; Rahe et al., 1998; Kawakata et al., 2000). Stepovers may be inherited from the earliest stages of fault development (Kawakata et al., 2000), and then appear to evolve with time. In the incipient stage, the pull-apart is defined primarily by high-angle basin-bounding normal faults; with continued strike-slip, more normal faults form, and at the most mature stages, through-going, strike-slip transfer faults form, which may limit extension (Rahe et al., 1998). Many features of the analog models appear to be identifiable with real examples (McClay and Dooley, 1995). The Hayward-Rodgers Creek pull-apart basin most resembles the incipient stage identified in analog models because there is little evidence for multiple normal faults or strike-slip transfer faults (Figs. 5,6) (Jachens et al., 2002). The locations of active pull-aparts may have migrated around San Pablo Bay, since the area of the gravity low (and presumably basin deposits) is much broader than the region currently caught between the overlapping Hayward and Rodgers Creek faults; migration of an active pull-apart was also proposed for the Dead Sea basin (ten Brink and Ben-Avraham, 1989). The Hayward-Rodgers Creek pull-apart may also be asymmetric, since there is a more pronounced basin boundary on the north edge than to the south (Fig. 5).

Could an earthquake rupture through the Hayward-Rodgers Creek stepover?

A key question addressed by this study is whether structure within the Hayward-Rodgers Creek fault stepover enables an earthquake to rupture through. We have concluded that the two faults overlap across much of San Pablo Bay, and that there is likely no transfer fault that connects them. In addition, our cross-section (Fig. 2) across south San Pablo Bay, and those of Wright and Smith (1992) all show the Rodgers Creek fault dipping steeply down to the northeast, away from the Hayward fault, suggesting that the two faults probably do not converge at depth. A strike-slip link between the two faults that could facilitate through-going rupture does not appear to be present at the stepover.

The next question is whether the two faults are close enough such that a rupture propagating along one fault could jump to the other through dynamic stress transfer. This study shows that at the surface, the Hayward and Rodgers Creek faults are as close as 4 km away from one another in San Pablo Bay, 2 km closer than was previous thought. The two faults are an average 5 km apart if dips are projected through seismogenic depths. The critical offset distance for an earthquake to jump through a dilatational stepover is about 4-5 km, based on observations and numerical modeling (Barka and Kandinsky-Cade, 1988; Harris, 1992; Harris and Day, 1993; 1999; Lettis et al., 2002). The 4-5 km gap between the Hayward and Rodgers Creek faults means that it might be possible for an earthquake to rupture through the stepover, though to do so would require both faults to be at a high state of failure stress (Harris and Day, 1999).

A consequence of no connecting strike-slip fault between the Hayward and Rodgers Creek faults within the stepover is that extensional strain must be accommodated in the intervening crust (Fig. 8). We inferred a high-angle normal (or oblique) fault near the northern termination

of the Hayward fault in San Pablo Bay based on gravity (Fig. 5), and analogous pull-apart structures. Numerical models show that transfer of strike-slip rupture onto an orthogonal strike-slip fault is rapidly extinguished, particularly if the orthogonal fault lies near the end of the initial rupture (Kase and Kuge, 1998). However, it is not possible to rule out a linked strike-slip and orthogonal normal fault earthquake passing through the stepover; multi-segment ruptures facilitated by connecting orthogonal faults are observed in thrust and strike-slip systems (e.g., Magistrale and Day, 1999). To gain more insight into this possibility, we investigate the only known **M**≥6 earthquake to have occurred at or near the Hyaward-Rodgers Creek stepover to determine its location and mechanism.

Normal faulting within the Hayward-Rodgers Creek stepover? The 1898 Mare Island earthquake revisited

An earthquake struck the northern San Francisco bay area on March 30, 1898, causing significant damage around north San Pablo Bay, particularly on Mare Island (Toppozada et al., 1992). Aftershocks were felt in regions mostly north of San Pablo Bay, consistent with a Rodgers Creek fault source for the 1898 quake (Toppozada et al., 1992). The intensity center was located in northeast San Pablo Bay by Toppozada et al. (1992) and Bakun (1999), who suggested that the **M**=6.0-6.5 event could have occurred on the southern Rodgers Creek fault, the north Hayward fault, or on a blind thrust east of Mare Island. We calculate a similar location for the intensity center using modified Mercalli intensity (MMI) values compiled by Toppazada et al. (1992) using the technique of Bakun and Wentworth (1999) (Fig. 10).

The 1898 earthquake may have produced small tsunami and seiche resulting from coseismic vertical deformation of the Bay floor. Lander et al. (1993) and Toppozada et al. (1992) provide

several newspaper descriptions indicating a small tsunami: The Evening Bee (March 31, 1898, p. 2) "Out on the Bay a violent tidal wave lifted small boats high upon its crest …"; The Record Union (March 31, 1898, p. 8) "The waters of San Francisco Bay rose in a tidal wave two feet high (0.6 m), but almost immediately subsided"; The San Francisco Call (April 3, 1898, p. 5) "Sonoma Creek kicked up its heels and ran up its banks until it flooded all the land unprotected by levees, and in some it even splashed over these, something it has never done before." From these and other reports, it appears that the1898 earthquake may have produced coseismic vertical motion of the Bay floor, generating a small tsunami.

Coseismic displacement of the San Pablo Bay floor

We investigated historical hydrographic surveys of San Pablo Bay to evaluate any vertical bay-floor displacement associated with the 1898 earthquake. From 1856 to 1951, the US Coast and Geodetic Survey and the National Ocean Service made 5 surveys of San Pablo Bay. Depth change between surveys is the result of sedimentation (accretion and erosion) and, potentially, tectonic movement. We determined depth change before and after the 1898 earthquake in two areas, one between the Rodgers Creek and Hayward faults and one east of the Rodgers Creek fault (Fig. 11). Both ~4-km^2-areas encompass similar depth ranges (between mean lower low water (MLLW) and 4 feet below MLLW), and are located away from streams where high deposition rates and spatial gradients have been observed (Jaffe et al., 1998). We were limited in our choice of areas by the distribution of pre- and post earthquake surveys. The 1890s survey was made before (as early as July 1896) and after (there were several days of surveying as late as 1901) the 1898 earthquake. The shallow area within the stepover was chosen because a post-earthquake survey was also conducted there in 1898. Soundings and contours for each survey

were digitized and interpolated to generate a continuous bathymetric surface (Jaffe et al., 1998). The resultant grids were supported by hundreds of depth soundings within our area of interest (Fig. 11). After correcting for datum changes between surveys, the grids were differenced to calculate depth change over time.

To ensure accuracy of depth soundings, the US Coast and Geodetic Survey verified depth values during data collection. At the time of the 1898 earthquake, the accuracy standard for depths shallower than 1.52 m was 0.08 m (Schallowitz, 1964). Comparison of individual soundings from different surveys can detect depth changes of 0.15 m. However, average depth change for the analyzed areas, which are based on numerous soundings (Fig. 11), are significant at less than 0.15 m because sounding errors tend to be random and are partially averaged out.

The time series of differential depth change within and outside of the Hayward-Rodgers Creek stepover shows that the area between the faults either dropped or was erosional near the time of the 1898 earthquake (Fig. 11). The sedimentation signal must be removed to determine whether depth change was caused by tectonic movement or erosion. Surveys before (1856 and 1887) and after (1922 and 1951) the 1898 earthquake establish sedimentation trends. From 1856 to 1887, the area within the stepover had ~0.4 m more deposition than the area east of the faults. This difference decreased through time to less than 0.05 m during the period from 1922 to 1951. This difference is expected to decrease over time because of diminishing sediment delivery from local streams and the San Francisco Delta (Gilbert, 1917; Smith, 1965). The ~0.3 m difference in the period directly after the earthquake (from the 1890s to 1922) (Fig. 11) is larger than expected based upon sediment delivery considerations. This is consistent with the 1898 earthquake displacing the area between the faults deeper than the equilibrium profile, causing an increase in deposition to reestablish equilibrium. Based on sediment delivery and depth change

difference during non-earthquake periods, the area between the faults was between 0.1 and 0.3 m more depositional than the area to the east of the faults from 1887 to the 1890s. Accounting for this difference, there was between 0.6 and 0.8 m of average downward vertical displacement from the 1898 earthquake in one region (Fig. 11) of northern San Pablo Bay between the Rodgers Creek and Hayward faults.

Given that the Hayward-Rodgers Creek fault stepover geometry is expected to produce extensional deformation, logical mechanisms for vertical Bay-floor deformation might be oblique slip on one of the strike-slip faults, or dip slip on a normal fault. We tested some simple scenarios for the 1898 earthquake to determine how much of a dip-slip component would be required to produce an observable tsunami, and be consistent with observed Bay floor displacement.

Hydrodynamic modeling

During an earthquake, coseismic vertical displacement of the sea floor creates a gravitational instability in the water column that generates a tsunami. Because of the large wavelength of the coseismic displacement field, the length of the initial tsunami wave is nearly identical to the displacement at the sea floor. Only when the wavelength of displacement is less than about 3 times the water depth, or in regions of very steep bathymetry, do special modifications need to be made in approximating the initial tsunami wavefield to the vertical coseismic displacement. During propagation, the gravitational potential energy is transferred to kinetic energy, such that the wave travels at a long-wave phase velocity of $c = \sqrt{gh}$, where g is the gravitational acceleration and h is the water depth in meters. The large wavelength of tsunamis also permits

us to use the following shallow-water-wave equations to describe the evolution of the tsunami during propagation:

$$\frac{\partial(\zeta + h)}{\partial t} + \nabla \bullet [\mathbf{v}(\zeta + h)] = 0 \tag{2}$$

and

$$\frac{D\mathbf{v}}{Dt} + g\nabla\zeta + \tau\mathbf{v} = 0 \tag{3}$$

where ζ is the water-surface elevation, $\mathbf{v}$ is the depth-averaged horizontal-velocity field, and τ is a bottom-friction coefficient (Cheng et al., 1993). The substantial derivative is given by

$$\frac{D}{Dt} = \frac{\partial}{\partial t} + (\mathbf{v} \bullet \nabla) \ . \tag{4}$$

To model the tsunami from the 1898 earthquake, we used a modified (Geist and Zoback, 1999) version of the TRIM (tidal, residual, intertidal mudflat) shallow-water-circulation model of Casulli (1990) and Cheng et al. (1993) that has been extensively used to study tidal and residual circulation in San Francisco Bay.

Assuming incompressibility in the water column, initial conditions are specified by the vertical coseismic displacement field calculated from elastic-dislocation theory (Okada, 1992), using different source parameters for the 1898 earthquake. The water-depth-dependent bottom-friction coefficients are the same as those described by Cheng et al. (1993). One particular advantage of the TRIM model is that the emergence and flooding of shallow and low-lying areas

are properly accounted for (Cheng et al., 1993). The grid spacing for the model is 250 m, corresponding to the gridded bathymetry available for San Francisco Bay most recently used by McDonald and Cheng (1997). A 18-s time interval was used to model the evolution of the tsunami.

1898 earthquake tsunami modeling results

Simulations of potential 1898 earthquake sources were run on pure strike-slip, oblique strike-slip and pure normal-slip faults. Only high-angle (34˚-70˚ dip) pure-normal slip sources produced enough vertical Bay-floor deformation to generate a measurable tsunami in the model. We located the source fault along the southwest-northeast trending gravity gradient in north San Pablo Bay evident in Figure 5, which is not far from the calculated intensity center for the 1898 earthquake (Fig. 10). The potential fault is relatively short at ~6 km in length, and could generate a M~6 normal fault event if the rupture surface was ~18 km wide with about .35 m average slip (Wells and Coppersmith, 1994).

Maximum modeled wave height from the 1898 tsunami model was about 0.1 m (Fig. 12), well short of the reported ~0.6 m height. However, only a pure dip-slip mechanism produced any modeled tsunami at all; we thus conclude that, if the reports of tsunami activity are valid, the 1898 earthquake most likely had a strong dip-slip component. The lack of significant relief on the Bay floor and very shallow water depth make a coseismic landslide-induced cause for the tsunami very unlikely. We modeled the 1898 event with a uniform slip distribution; heterogeneous slip might concentrate or alter the maximum wave height (Geist, 2002), offering one explanation for the discrepancy between modeled and reported wave height. Unfortunately, no quantitative measure of the tsunami is available because storm activity obscured the marigram for a several-day period around the earthquake (Lander et al., 1993).

One geographic convergence between the model results and historical reports following the 1898 event occurs at Sonoma Creek. Flooding of lowlands adjacent to the creek of a style not previously observed happened after the earthquake. The hydrodynamic model shows at least two relatively high-amplitude waves concentrating at the mouth of Sonoma Creek, one at t=0.9 hours and the other at t=2.8 hours following the earthquake (Fig. 12).

In summary, because of the Hayward-Rodgers Creek fault geometry, the crust between the faults is expected to undergo significant extensional strain, probably on southwest-northeast trending normal faults. Quantitative and anecdotal observations following the 1898 earthquake suggest that vertical Bay-floor deformation may have caused a small tsunami. We conclude from modeling different 1898 rupture scenarios, that only a dip-slip mechanism could have produced an observable tsunami. Finite-element modeling indicates that the extensional stressing rate within the fault stepover would cause normal-fault earthquakes on 50-500-year intervals depending on stress drop. Normal events within the stepover are expected after large strike-slip events on either the Hayward or Rodgers Creek faults. If the 1898 event is interpreted as the last normal-fault event, then it may be some time before another such event occurs. In at least the 1898 case, the normal fault appears to have ruptured as an independent event rather than as part of a larger multi-segment earthquake.

Conclusions

We studied the dilatational Hayward-Rodgers Creek fault stepover beneath San Pablo Bay with a variety of techniques to better understand fault geometry and mechanics. We overlaid high-resolution seismic reflection data onto a tomographic seismic velocity model yielding a structural cross-section of the upper ~2 km of the crust in south San Pablo Bay. This section, when combined with sections across central and north San Pablo Bay (Wright and Smith, 1992),

allows us to determine the southern extent of the Rodgers Creek fault, and its closest approach to the Hayward fault (~4 km). Thus an earthquake could feasibly jump the stepover, though only if both fault segments were in a state of high failure stress (Barka and Kandinsky-Cade, 1988; Harris, 1992; Harris and Day, 1993; 1999).

The Rodgers Creek fault dips away from the Hayward fault on all three structural cross sections in San Pablo Bay, and we conclude that the two faults probably do not join at depth. Interpretation of aeromagnetic data in the region suggests that a transfer fault or other connecting strike-slip structure between the Hayward and Rodgers Creek faults is unlikely. The lack of such a structure implies that slip on the Hayward and Rodgers Creek faults should produce a pull-apart basin in the stepover. Interpretation of filtered gravity data in the region demonstrates consistency with our fault map in that a relative gravity low appears to correlate with the area between the Hayward and Rodgers Creek faults. Further interpretation of gravity data suggests that a southwest-northeast trending boundary across north San Pablo Bay may correspond to a normal fault. A finite element model of the Hayward-Rodgers Creek stepover allows us to calculate the differential stressing rate in the crust between the two strike-slip faults. We find that the present fault configuration could persist with disconnected slip on the Hayward and Rodgers Creek faults for about 10-20 ky before frictional strength in the stepover zone is overcome. After the crust is broken, the rate of extensional earthquakes in the stepover is expected to be one 1-10 MPa stress-drop event every 50-500 years.

To gain insight into the mechanics of the Hayward-Rodgers Creek stepover, we re-examined the **M**=6.0-6.5 1898 Mare Island earthquake that occurred somewhere in north San Pablo Bay. The event was associated with a reported small tsunami, and hydrographic measurements made before and after the 1890's indicate anomalous subsidence of the Bay floor within the stepover

compared with other periods. A tsunami is produced mainly by vertical displacement of the sea floor, and we thus examined a number of different rupture scenarios. We concluded that if the anecdotal accounts of tsunami activity are correct, then the 1898 earthquake was probably a normal fault rupture in north San Pablo Bay. Normal faulting within the stepover poses a dual hazard of independent **M**~6 earthquakes as well as potentially linking continuous rupture of the Hayward and Rodgers Creek faults.

Acknowledgements This paper benefited significantly from comments by Bill Bakun, David Oglesby, Uri ten Brink, Tousson Toppozada, Mary Lou Zoback, and one anonymous reviewer. George Meyers of the National Oceanic and Atmospheric Administration in Silver Springs, Maryland assisted in determining exact dates of soundings from historical hydrographic surveys.

References

Anima, R. J., P. L. Williams, and J. McCarthy (1992). High resolution marine seismic reflection profiles across east Bay faults in *Proc. of the Second Conference on Earthquake Hazards in the Eastern San Francisco Bay Area,* G. Borchardt, S. E. Hirschfeld, J. J. Lienkaemper, P. McClellan, and I. G. Wong (Editors), *Calif. Div. Mines Geol. Spec. Publ. 113*,, p. 18.

Bakun, W. H., (1999). Seismic activity of the San Francisco Bay region, Bull. Seismol. Soc. Am., 89, 764-784.

Bakun , W. H., and C. M. Wentworth (1997). Estimating earthquake location and magnitude from seismic intensity data, *Bull. Seismol. Soc. Am. 87*, 1502-1521.

Barka, A. A., and K. Kandinsky-Cade (1988). Strike-slip fault geometry in Turkey and its influence on earthquake activity, Tectonics, 7, 663-684.

Ben-Avraham, Z., and M. D. Zoback (1992). Transform-normal extension and asymmetric basins: An alternative to pull-apart models, Geology, 20, 423-426.

Bird, P., and X. Kong, (1994). Computer simulations of California tectonics confirm very low strength of major faults, Geol. Soc. Am. Bull., 106, 159-174.

Blakely, R. J., (1995). Potential theory in gravity and magnetic applications, Cambridge, Cambridge University Press, 441 pp.

Bruns, T., et al., (2002). in T. Parsons (editor), Crustal structure of the coastal and marine San Francisco Bay region, U. S. Geological Survey Professional Paper, 1658, in press.

Casulli, V., (1990). Semi-implicit finite difference methods for the two-dimensional shallow water equations: Journal of Computational Physics, v. 86, p. 56-74.

Cheng, R.T., Casulli, V., and Gartner, J.W., (1993). Tidal, residual, intertidal mudflat (TRIM) model and its applications to San Francisco Bay, California: Estuarine, Coastal and Shelf Science, v. 36, no. 3, p. 235-280.

Childs, J. R., Hart, P. E., Sliter, R, Bruns, T. R., and Marlow, M., (2000). High-resolution marine seismic reflection data from the San Francisco Bay area: 1993-1997, U.S. Geological Survey Open File Report, 00-494.

Geist, E. L., (2002). Complex earthquake rupture and local tsunamis, J. Geophys. Res., 107, 10.1029/2000JB000139.

Geist, E. L., and D. J. Andrews, (2000). Slip rates on San Francisco Bay area faults from anelastic deformation of the continental lithosphere, J. Geophys. Res., 105, 25543-25552.

Geist, E. L., and Zoback, M. L. (1999). Analysis of the tsunami generated by the M_W 7.8 1906 San Francisco earthquake:, Geology, 27, 15–18.

Gilbert, G. K., (1917). Hydraulic mining debris in the Sierra Nevada, U. S. Geological Survey Professional Paper, 105, 154 p.

Harris, R. A., (1992). Dynamic interaction of parallel strike-slip fault-segments: Some implications for the eastern San Francisco Bay area, in *Proc. of the Second Conference on Earthquake Hazards in the Eastern San Francisco Bay Area,* G. Borchardt, S. E. Hirschfeld, J. J. Lienkaemper, P. McClellan, and I. G. Wong (Editors), *Calif. Div. Mines Geol. Spec. Publ. 113*,, 73-80.

Harris, R. A., and S. M. Day (1993). Dynamics of fault interaction: Parallel strike-slip faults, J. Geophys. Res., 98, 4461-4472.

Harris, R. A., and S. M. Day, (1999). Dynamic 3D simulations of earthquakes on en echelon faults, Geophys. Res. Lett., 26, 2089-2092.

Jachens , R. C. et al., (2002). in T. Parsons (editor), Crustal structure of the coastal and marine San Francisco Bay region, U. S. Geological Survey Professional Paper, 1658, in press.

Jaffe, B. E., R. E. Smith, and L. Torresan, (1998). Sedimentation and bathymetric change in San Pablo Bay, 1856-1983, U.S. Geological Survey Open-File Report, 98-759.

Kase, Y., and K. Kuge (1998). Numerical simulation of spontaneous rupture processes on two non-coplanar faults: the effect of geometry on fault interaction, Geophys. J. Int., 135, 911-922.

Kawakata, H., A. Cho, T. Yanagidani, and M. Shimada (2000). Gross structure of a fault during its formation process in Westerly granite, Tectonophysics, 323, 61-76.

Lachenbruch, A. H., and J. H. Sass, (1980). Heat flow and energetics of the San Andreas fault zone, J. Geophys. Res., 85 6185-6222.

Lander, J. F., P. A. Lockridge, and M. J. Kozuch (1993). Tsunamis affecting the west coast of the United States 1806-1992, NGDC Key to Geophysical Records Documentation No. 29, National Oceanic and Atmospheric Administration, Boulder, CO.

Langel, R. A., (1992). International Geomagnetic Reference Field, 1991 revision, Geophysics, 57, 956-959.

Lees, J. M., and R. S. Crosson, (1989). Tomographic inversion for three-dimensional velocity structure at Mount St. Helens using earthquake data, J. Geophys. Res., 94, 5716-5728, 1989.

Lettis, W., J. Bachhuber, R. Witter, C. Brankman, C. E. Randolph, A. Barka, W. D. Page, and A. Kaya, (2002). Influence of releasing step-overs on surface fault rupture and fault segmentation: Examples from the 17 August 1999 Izmit earthquake on the North Anatolian fault, Turkey, Bull. Seismol. Soc. Am., 92, 19-42.

Magistrale, H., and S. Day, (1999). 3D simulations of multi-segment thrust fault rupture, Geophys. Res. Lett., 26, 2093-2096.

Mann, P., M. Hempton, D. Bradley, and K. Burke, (1983). Development of pull-apart basins, J. Geol., 91, 529-554.

McClay, K. and T. Dooley (1995). Analogue models of pull-apart basins, Geology, 23, 711-714.

McDonald, E.T., and Cheng, R.T., (1997). A numerical model of sediment transport applied to San Francisco Bay, California: Journal of Marine Environmental Engineering, 4, 1-41.

Miller, S. A., (1996). Fluid-mediated influence of adjacent thrusting on the seismic cycle at Parkfield, Nature, 382, 799-802.

Morrow, C. A., and Lockner, D. A., (2001). Hayward fault rocks: Porosity, density and strength measurements, U. S. Geological Survey Open File Report, v. 01-421, 28pp.

Paige, C.C. and M.A. Saunders, (1982). LSQR: An algorithm for sparse linear equations and sparse least squares, Trans. Math. Software, 8, 43-71.

Parsons, T., J. McCarthy, W. M. Kohler, C. J. Ammon, H. M. Benz, J. A. Hole, and E. E. Criley, (1996). The crustal structure of the Colorado Plateau, Arizona: Application of new long-offset seismic data analysis techniques, Journal of Geophysical Research, v. 101, p. 11,173-11,194.

Parsons, T., R. S. Stein, R. W. Simpson, and P. A. Reasenberg, (1999). Stress sensitivity of fault seismicity: a comparison between limited-offset oblique and major strike-slip faults, J. Geophys. Res., 104, 20,183-20,202.

Rahe, B., D. A. Ferrill, and A. P. Morris (1998). Physical analog modeling of pull-apart basin evolution, Tectonophysics, 285, 21-40.

Reasenberg, P. A., and Simpson, R. W., (1992). Response of regional seismicity to the static stress change produced by the Loma Prieta earthquake, Science, 255, 1687-1690.

Schallowitz, A. L. (1964). Shore and sea boundaries. Vol. 2, Pub. 10-1, U. S. Dept. of Commerce, Coast and Geodetic Survey, U. S. Govt. Print Office, Washington.

Smith, B. J., (1965). Sedimentation in the San Francisco Bay system, Proceedings of the Interagency Sedimentation Conference, U. S. Dep. Agr. Misc. Pub. 970, 675-708.

Sylvester, A., (1988). Strike-slip faults, Geol. Soc. Am. Bull., 100, 1666-1703.

ten Brink, U. S., and Z. Ben-Avraham (1989). Anatomy of a pull-apart basin: Seismic reflection observations of the Dead Sea basin, Tectonics, 8, 333-350.

ten Brink, U. S., R. Katzman, and J. Lin (1996). Three-dimensional models of deformations near strike-slip faults, J. Geophys. Res., 101, 16205-16220.

Toppozada, T. R., G. Borchardt, C. L. Hallstrom, and L. G. Youngs (1992). 1898 "Mare Island" earthquake at the southern end of the Rodgers Creek fault, in *Proc. of the Second Conference on Earthquake Hazards in the Eastern San Francisco Bay Area,* G. Borchardt, S. E.

Hirschfeld, J. J. Lienkaemper, P. McClellan, and I. G. Wong (Editors), *Calif. Div. Mines Geol. Spec. Publ. 113*, 385-392.

Vidale, J. E., (1990). Finite-difference calculation of traveltimes in three dimensions, Geophysics, 55, 521-526, 1990.

Waldhauser, F., and W. L. Ellsworth (2002). Fault structure and mechanics of the Hayward fault, California, from double-difference earthquake locations, J. Geophys. Res., 107, 10.1029/2000JB000084.

Wells, D. L., and K. J. Coppersmith, (1994). New empirical relationships among magnitude, rupture length, rupture width, rupture area, and surface displacement, Bull. Seismol. Soc. Amer., 84, 974-1002.

Working Group on California Earthquake Probabilities, (1999). Earthquake probabilities in the San Francisco Bay region: 2000 to 2030 - a summary of findings, USGS Open-File Report 99-517.

Wright, T. L., and N. Smith, (1992). Right step from the Hayward fault to the Rodgers Creek fault beneath San Pablo Bay, in *Proc. of the Second Conference on Earthquake Hazards in the Eastern San Francisco Bay Area,* G. Borchardt, S. E. Hirschfeld, J. J. Lienkaemper, P. McClellan, and I. G. Wong (Editors), *Calif. Div. Mines Geol. Spec. Publ. 113*, 407-417.

Zoback, M. D., (1991). State of stress and crustal deformation along weak transform faults, Philo. Trans. R. Soc. London, A337, 141-150.

Figure Captions

Figure 1. Map of San Francisco and San Pablo Bay showing the major strike-slip faults, the location of the seismic cross-section discussed in this paper, and the earthquake epicenters in the Hayward-Rodgers Creek stepover.

Figure 2. A structural cross-section (upper 2 km) across south San Pablo Bay and the Hayward-Rodgers Creek stepover (see Fig. 1 for location). Seismic reflection data are overlain on a tomographic seismic velocity section. A significant lateral contrast is observed about 1 km east of the presently active trace of the Hayward fault, and may represent an older fault trace. Another fault ~4 km east of the active Hayward fault separates east-dipping from west-dipping bedding within a basin; this structure is located on the Rodgers Creek fault trend projected from two structural sections in central and north San Pablo Bay developed by Wright and Smith (1992). Sparse relocated earthquake hypocenters (Waldhauser and Ellsworth, 2002) are shown below with and without the Wright and Smith (1992) interpretation.

Figure 3. Fault map of San Pablo Bay based on the cross-sections of Wright and Smith (1992) (cross-section locations shown with black lines) and our new section in south San Pablo Bay (cross-section location shown with red line). We carry the Pinole fault offshore at least as far north as our cross-section, and we connect the Rodgers Creek fault as far south as our section.

Figure 4. Earthquake focal mechanisms from the NCSN catalog 1967-2002 located within the Hayward-Rodgers Creek fault stepover in San Pablo Bay.

Figure 5. Gravity map of the San Pablo Bay region. An upward continued (500 m) signal was subtracted from the data, which filters out the broader wavelength features and allows us to focus on the shallowest part of the crust. A simplified fault map is shown by the black lines, and gravity gradients are identified by the white dots. A broad gravity low characterizes San Pablo Bay, and a subtly lower anomaly appears to coincide with the region between the Hayward and Rodgers Creek faults. This low is truncated near the north edge of San Pablo Bay by a strong gravity gradient that might be a normal fault boundary of a pull-apart basin.

Figure 6. Aeromagnetic map of San Pablo Bay. The continuous magnetic high that trends across central San Pablo Bay between the Hayward and Rodgers Creek faults was interpreted by Jachens et al. (2002) as evidence for the lack of a strike-slip transfer fault across the stepover.

Figure 7. Finite element model of the elastic part of the Hayward-Rodgers Creek stepover (upper 15 km). The west edge of the model was moved at a 9-mm/yr rate past the fixed east edge. The model is shaded by the relative fault-parallel displacement.

Figure 8. Predicted differential stress after 20 ky of Hayward-Rodgers Creek fault slip from finite element modeling. Strong extensional stresses build in the crust between the strike-slip faults. Gray lines show the orientations of horizontal least principal stress (extension direction). If normal faults were to develop within the stepover, their expected orientation is perpendicular to the least principal stress directions.

Figure 9. Differential stressing rate within the Hayward -Rodgers Creek stepover predicted from finite element modeling. Three curves show the rates for different coefficients of friction of the strike-slip faults. In all cases the stressing rate is about 0.02 MPa/yr. The gray area on the plot shows the range of measured frictional strength of rocks near the Hayward fault (Morrow and Lockner, 2001).

Figure 10. Modified Mercalli Intensity (MMI) observations (Toppozada et al., 1992) and calculated moment magnitude and intensity center (Bakun and Wentworth, 1997) of the 1898 Mare Island earthquake, which was located somewhere within north San Pablo Bay (Bakun, 1999).

Figure 11. (A) Location of areas where historical hydrographic surveys were used to determine if the 1898 earthquake caused vertical bay-floor displacement. Depth soundings and contours from the 1890s within each shaded area are shown in the expanded views. (B) Difference in depth change in the shaded areas in A. A negative value is less deposition (more erosion) or downward vertical displacement in the area between the faults.

Figure 12. Time windows of modeled wave height and flow directions of a tsunami caused by a normal fault dislocation located near the north end of San Pablo Bay where the gravity gradient is observed in Figure 5. The dislocation corresponds to a M~6.0 earthquake. This model is most consistent with reports of tsunami waves in the Bay and flooding of Sonoma Creek (pulses are modeled near the Creek mouth at t=0.9 hours and t=2.8 hours after the earthquake).

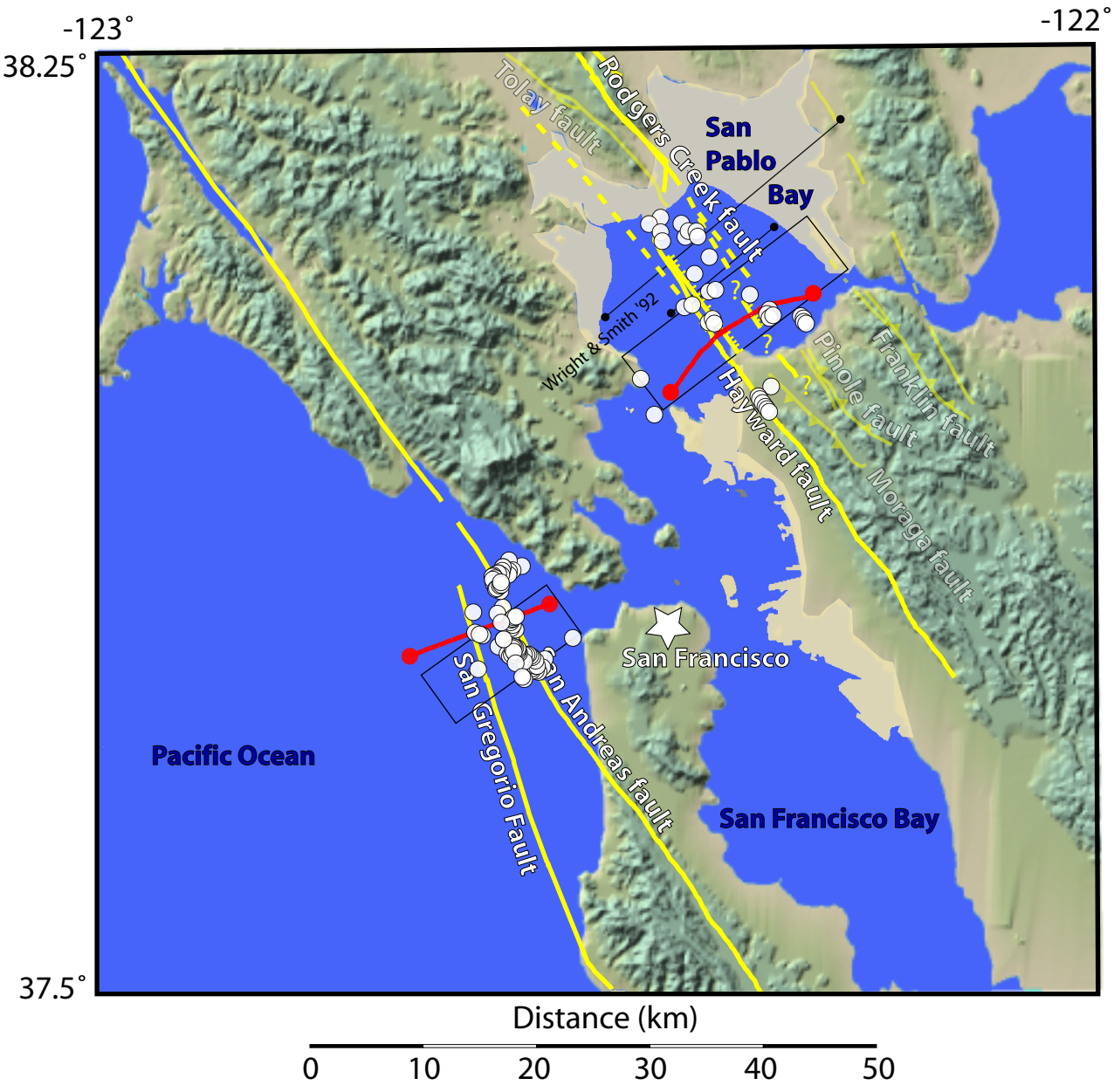
-123˚
-122˚
38.25˚
37.5˚
Tolay fault
Rodgers Creek fault
San
Pablo
Bay
Wright & Smith '92
Hayward fault
Pinole fault
Franklin fault
Moraga fault
San Francisco
San Gregorio Fault
San Andreas fault
Pacific Ocean
San Francisco Bay
Distance (km)
0
10
20
30
40
50

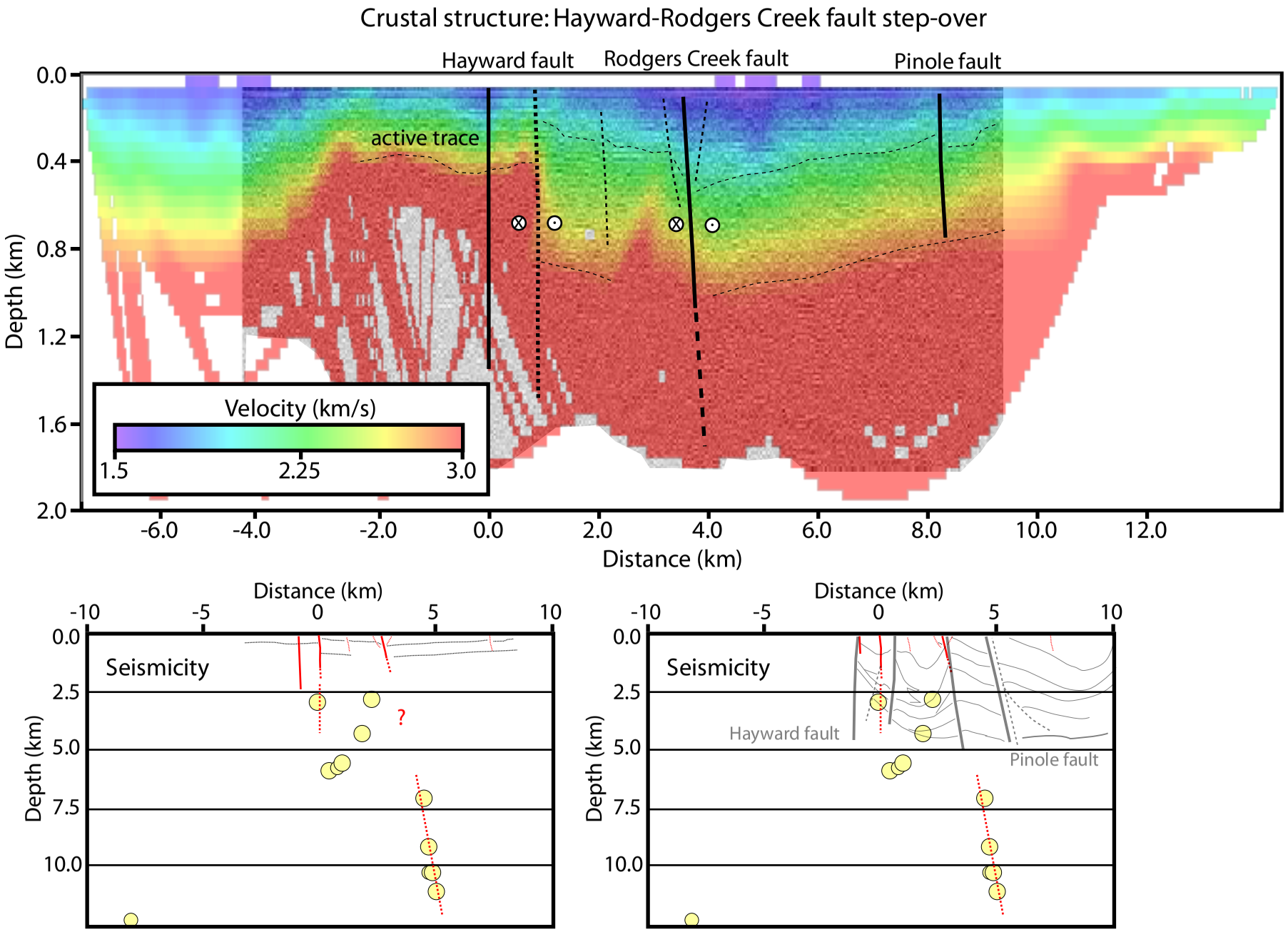
Crustal structure: Hayward-Rodgers Creek fault step-over
Hayward fault
Rodgers Creek fault
Pinole fault
active trace
Velocity (km/s)
1.5
2.25
3.0
Depth (km)
0.0
0.4
0.8
1.2
1.6
2.0
-6.0
-4.0
-2.0
0.0
2.0
4.0
6.0
8.0
10.0
12.0
Distance (km)
Distance (km)
-10
-5
0
5
10
Seismicity
?
Depth (km)
0.0
2.5
5.0
7.5
10.0
Distance (km)
Seismicity
Hayward fault
Pinole fault

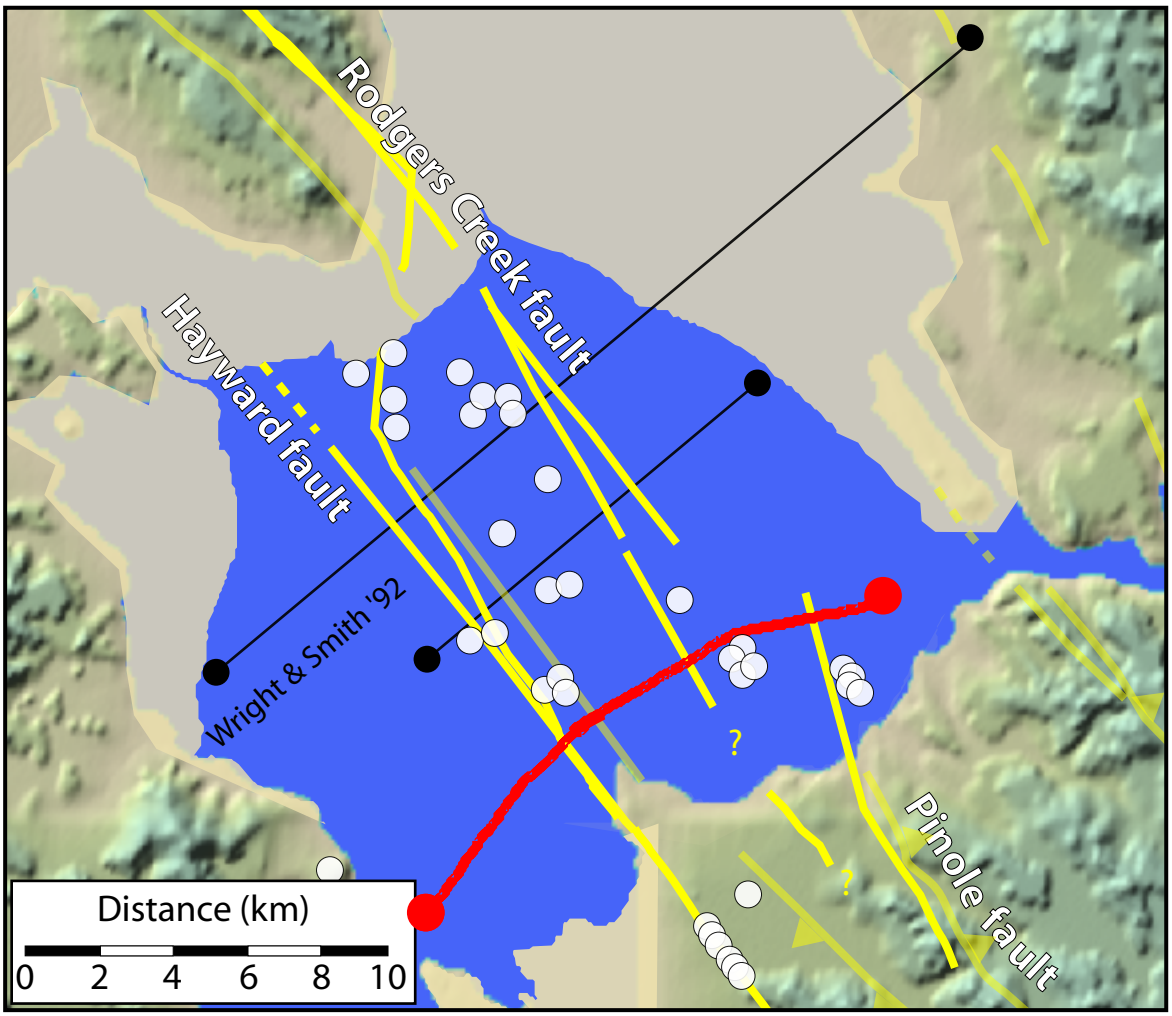
Rodgers Creek fault
Hayward fault
Wright & Smith '92
Pinole fault
?
?
Distance (km)
0 2 4 6 8 10

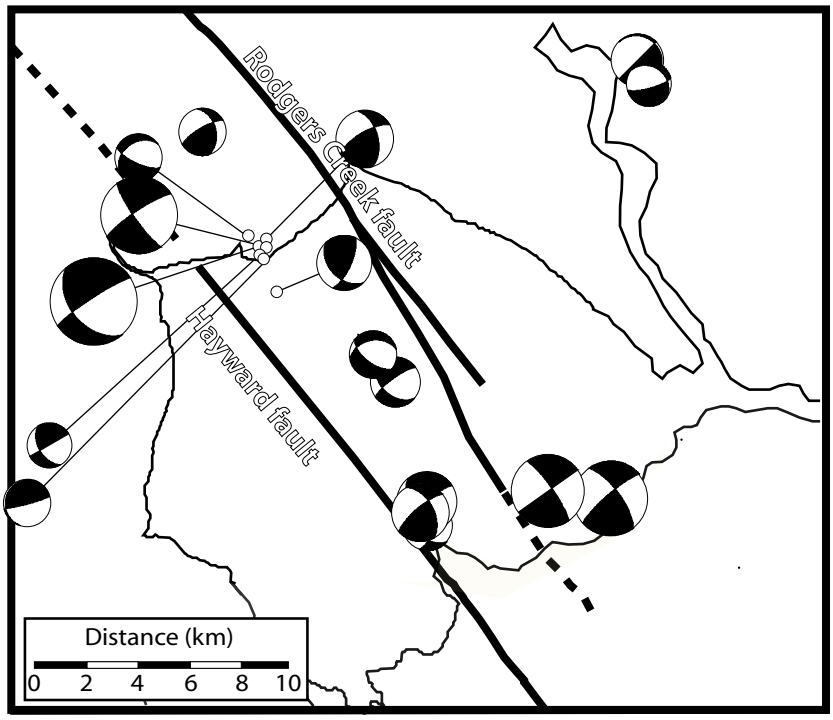
Rodgers Creek fault
Hayward fault
Distance (km)
0 2 4 6 8 10

Filtered gravity: Upward continued 500 m

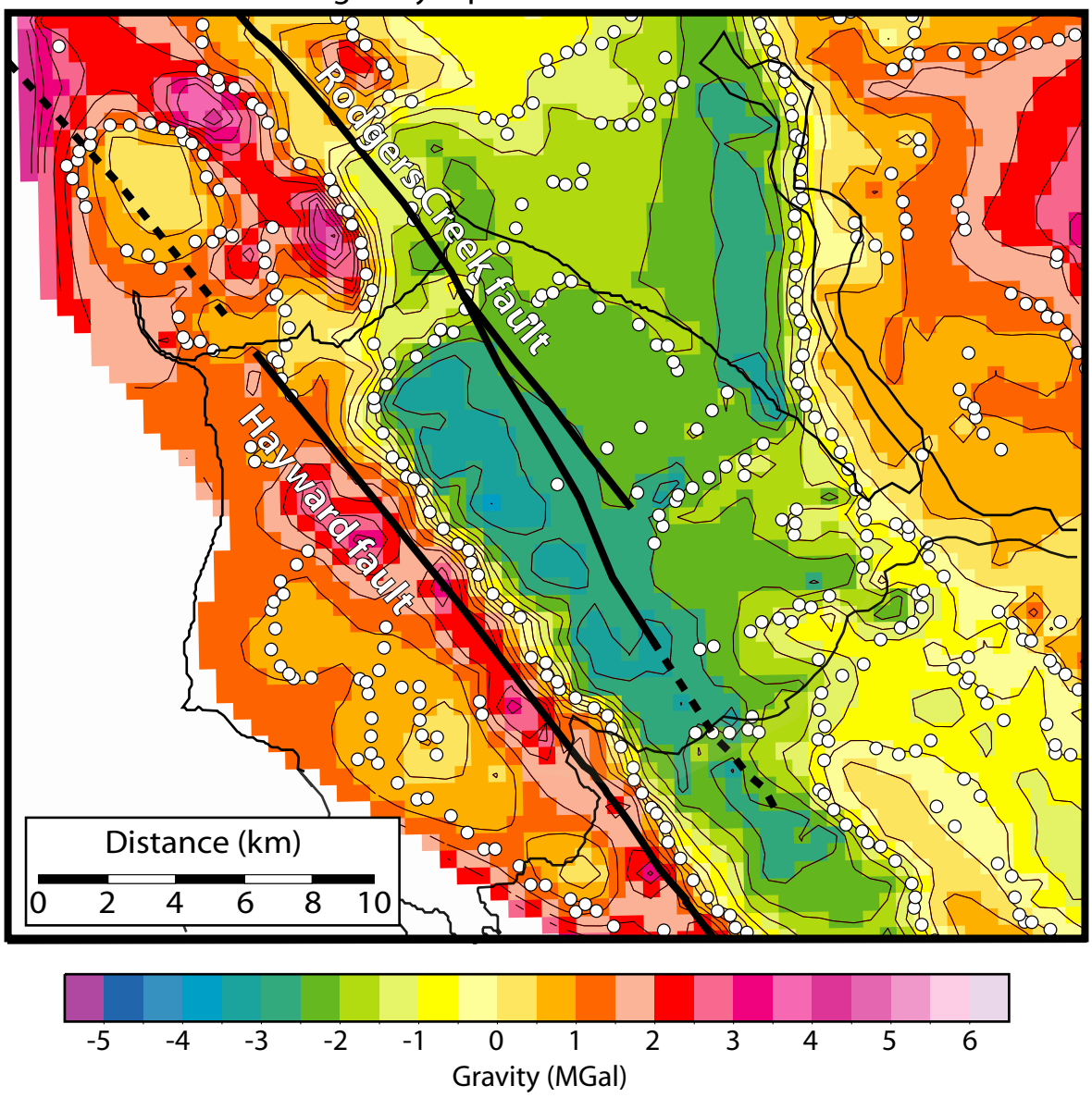

Magnetic Field

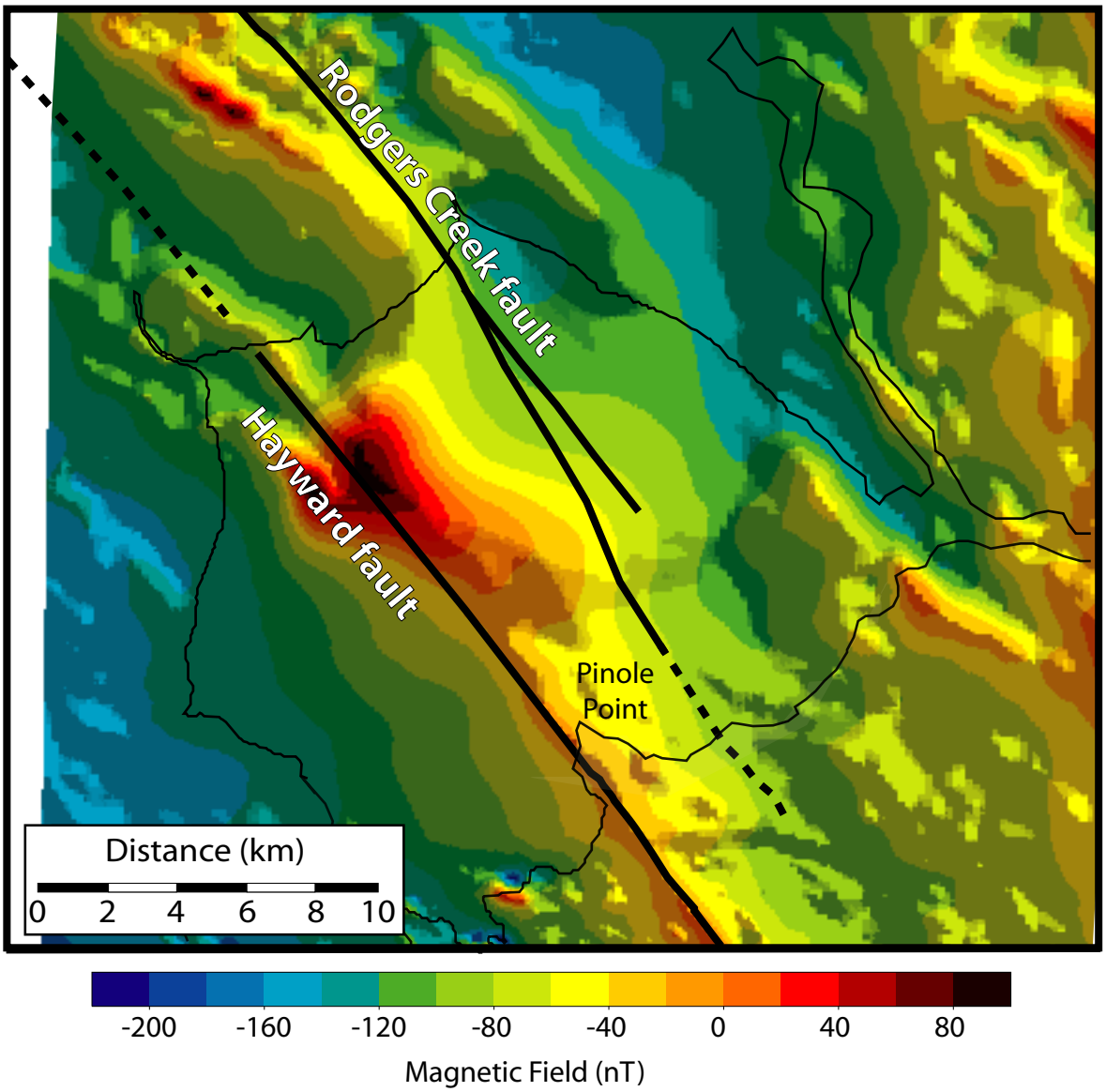

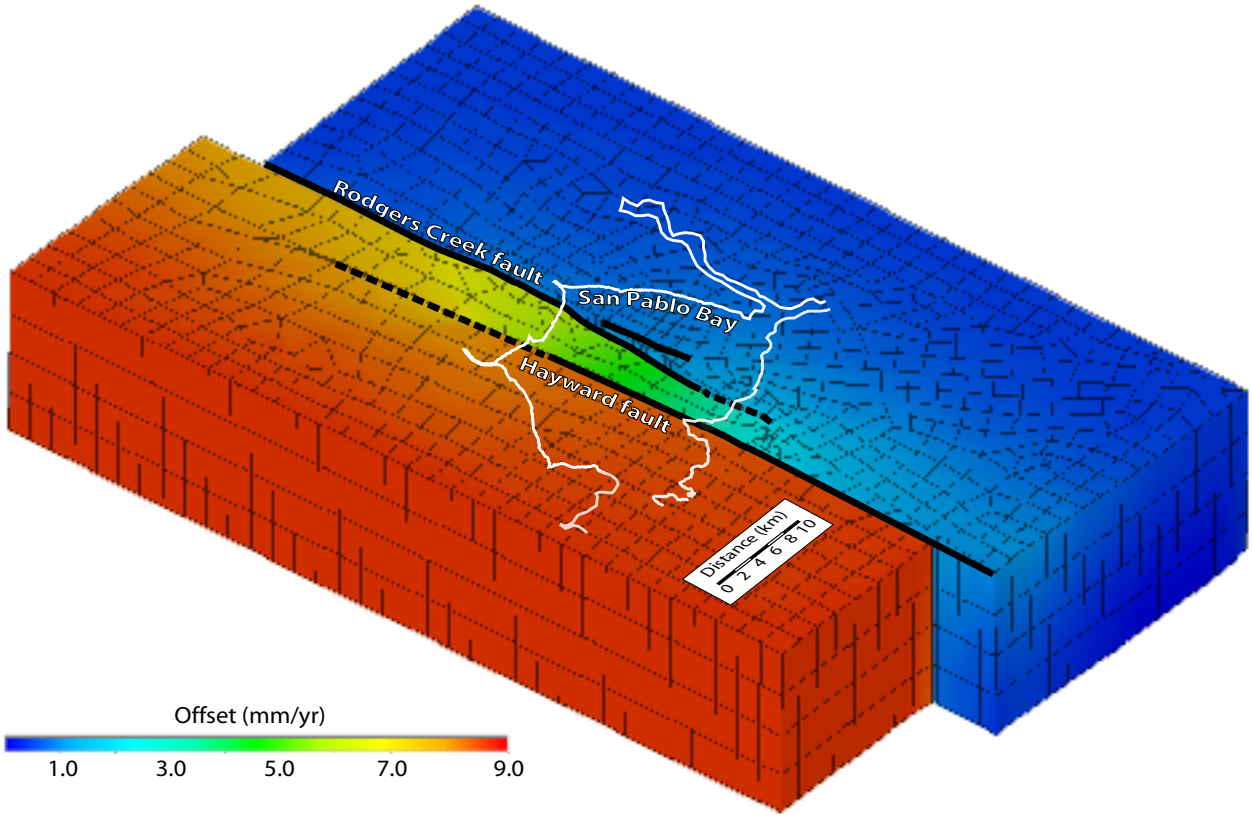
Rodgers Creek fault
San Pablo Bay
Hayward fault
Distance (km)
0 2 4 6 8 10
Offset (mm/yr)
1.0
3.0
5.0
7.0
9.0

Modeled differential stress and σ_3 orientations: Hayward-Rodgers Creek stepover

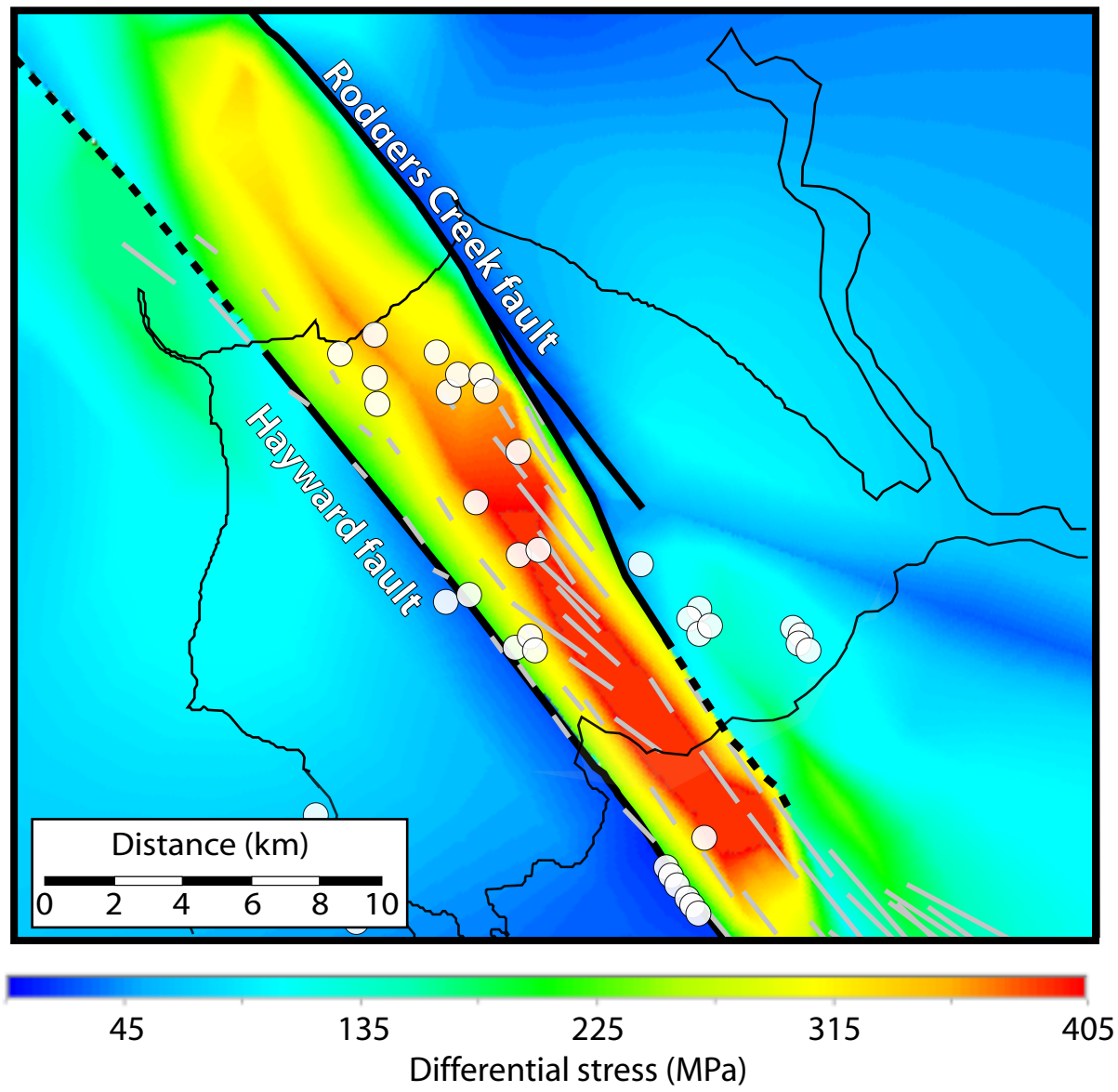

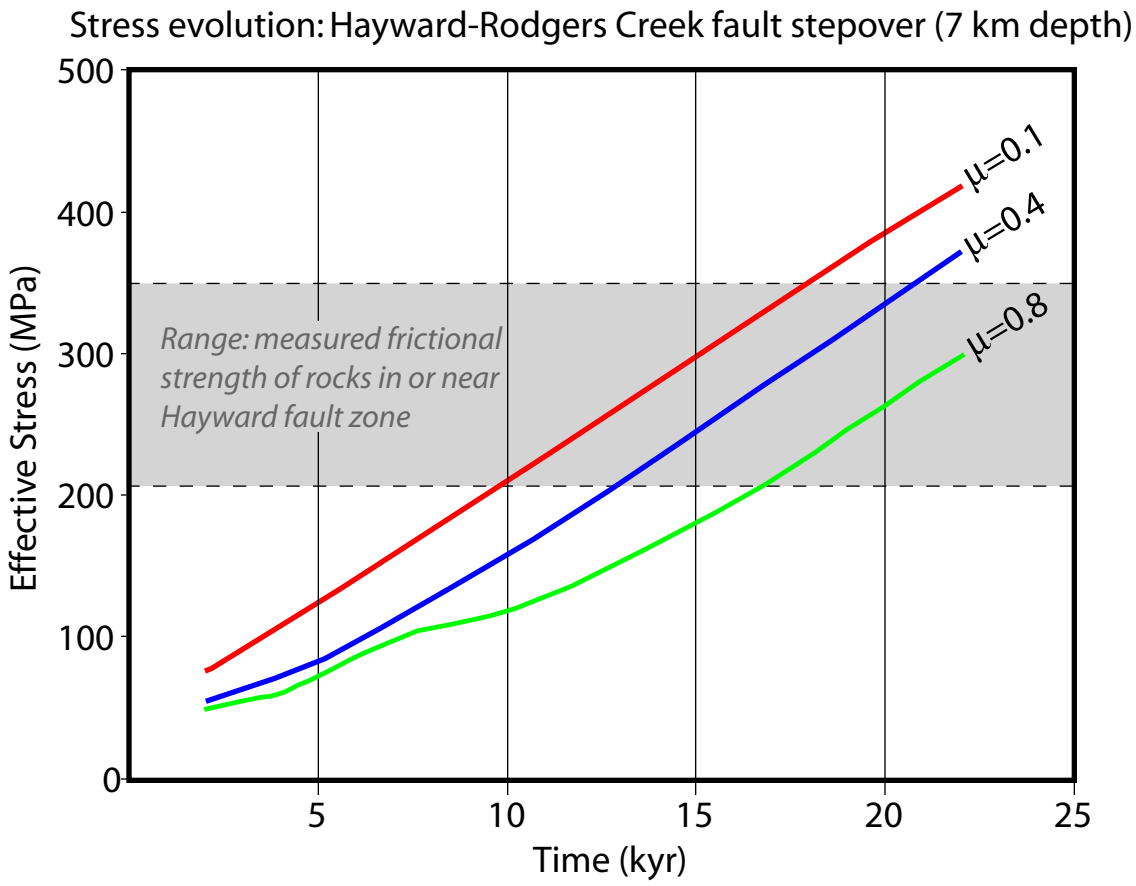
Stress evolution: Hayward-Rodgers Creek fault stepover (7 km depth)
Effective Stress (MPa)
500
400
300
200
100
0
5
10
15
20
25
Time (kyr)
μ=0.1
μ=0.4
μ=0.8
Range: measured frictional strength of rocks in or near Hayward fault zone

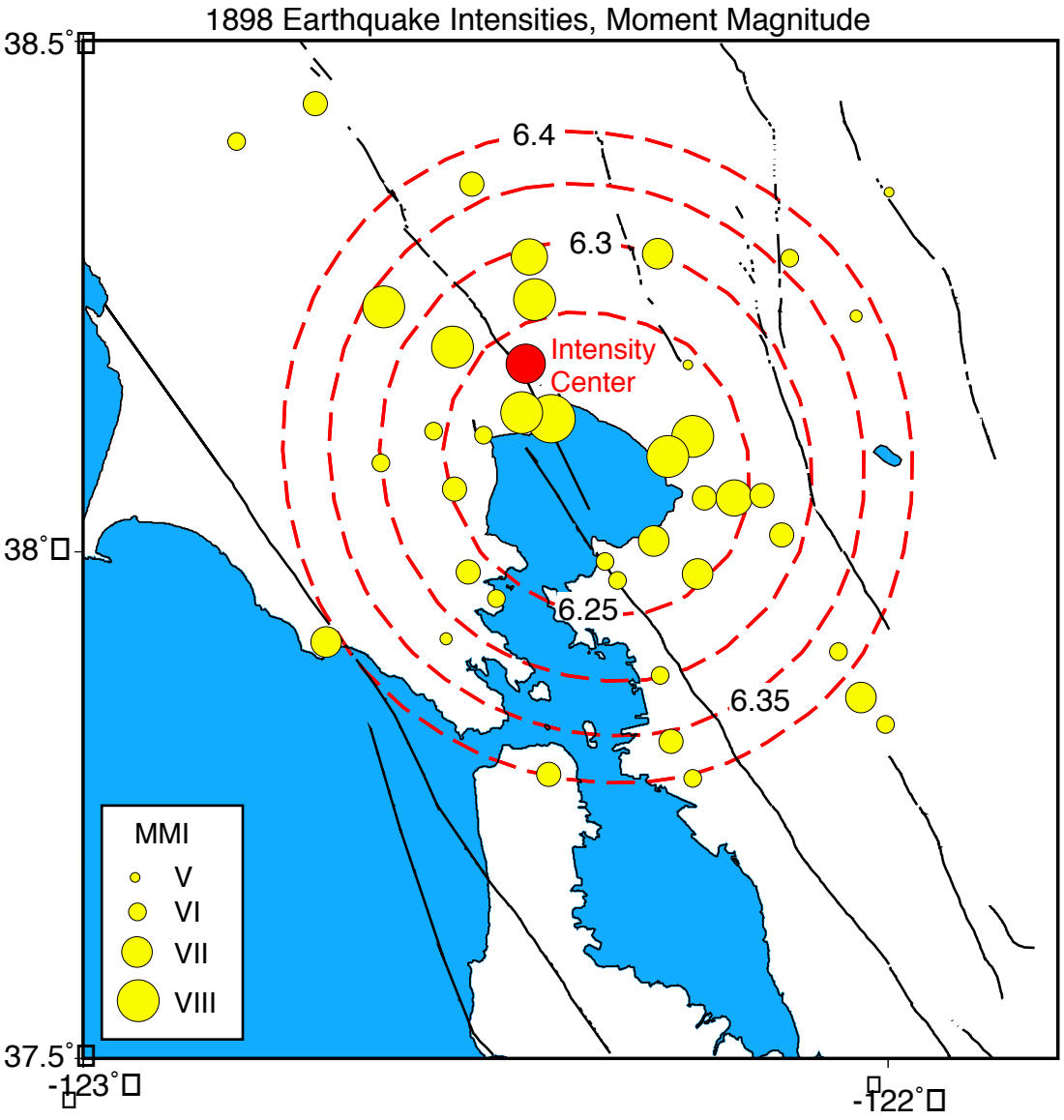
1898 Earthquake Intensities, Moment Magnitude
38.5°
38°
37.5°
-123°
-122°
6.4
6.3
6.25
6.35
Intensity
Center
MMI
V
VI
VII
VIII

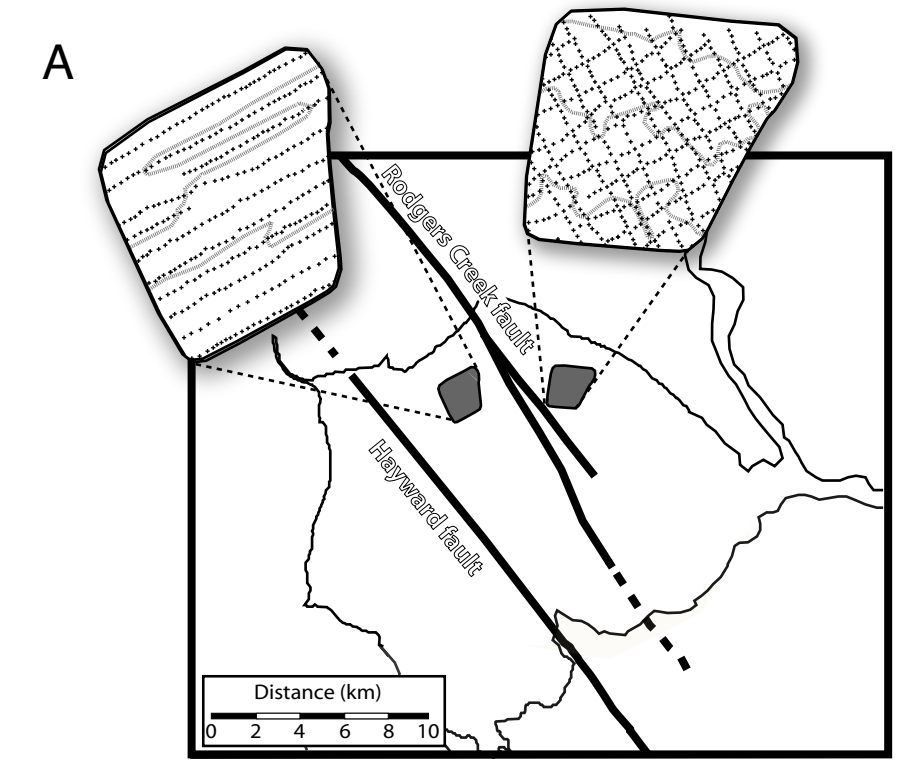
A
Rodgers Creek fault
Hayward fault
Distance (km)
0 2 4 6 8 10

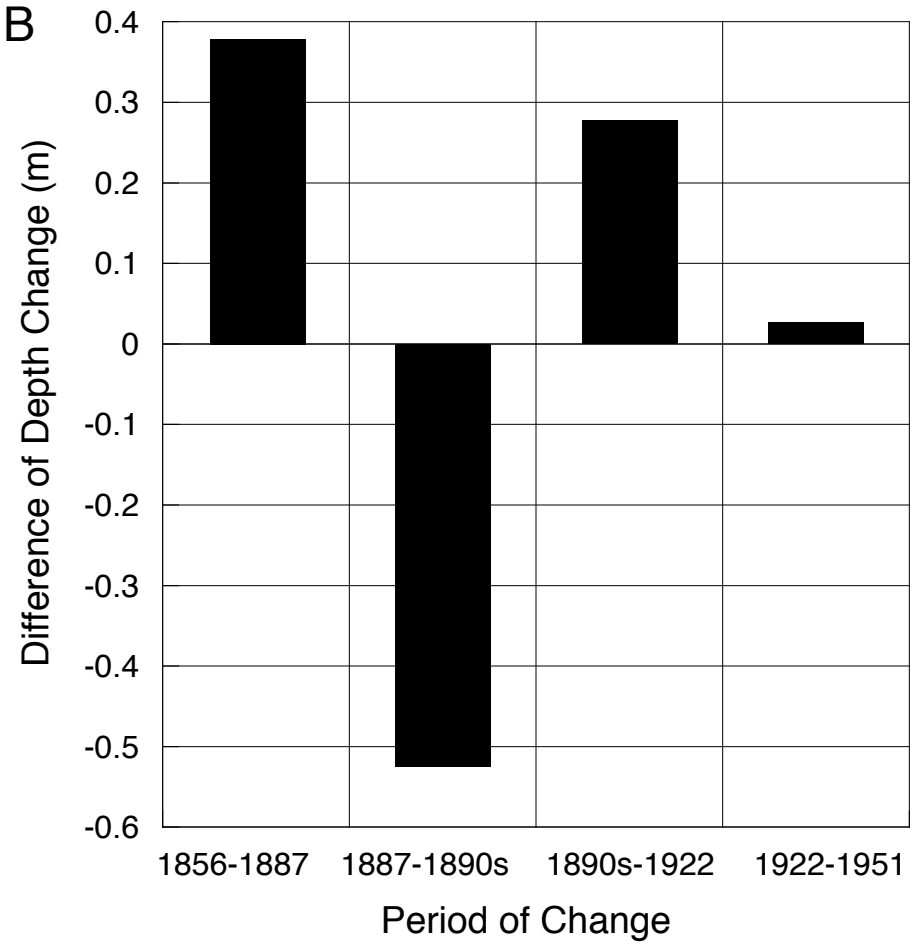
B
0.4
0.3
0.2
0.1
0
-0.1
-0.2
-0.3
-0.4
-0.5
-0.6
Difference of Depth Change (m)
1856-1887
1887-1890s
1890s-1922
1922-1951
Period of Change

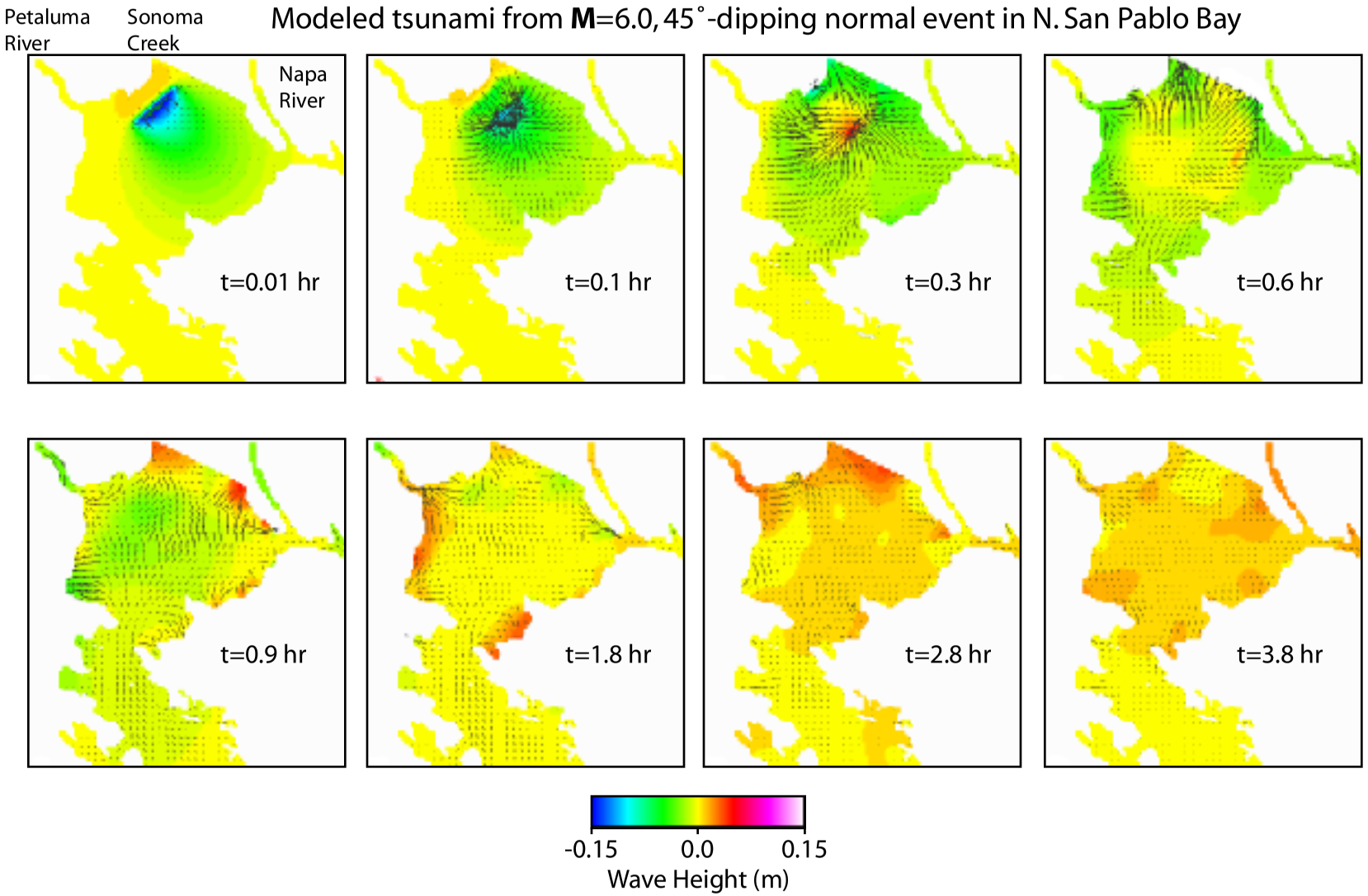
Petaluma River
Sonoma Creek
Modeled tsunami from **M**=6.0, 45˚-dipping normal event in N. San Pablo Bay
Napa River
t=0.01 hr
t=0.1 hr
t=0.3 hr
t=0.6 hr
t=0.9 hr
t=1.8 hr
t=2.8 hr
t=3.8 hr
-0.15
0.0
0.15
Wave Height (m)